DE GRUYTER
OPEN

Acta Geophysica
vol. 64, no. 3, June 2016, pp. 649-669
DOI: 10.1515/acgeo-2016-0023

Wavelet Characteristics of Hydrological and Dissolved Oxygen Time Series in a Lowland River

Agnieszka RAJWA-KULIGIEWICZ[1], Robert J. BIALIK[1,2], and Paweł M. ROWIŃSKI[1]

[1]Institute of Geophysics, Polish Academy of Sciences, Warszawa, Poland; e-mails: arajwa@igf.edu.pl (corresponding author), p.rowinski@igf.edu.pl

[2]Institute of Biochemistry and Biophysics, Polish Academy of Sciences, Warszawa, Poland; e-mail: rbialik@ibb.waw.pl

Abstract

In this study, we investigated the temporal variability of dissolved oxygen and water temperature in conjunction with water level fluctuations and river discharge in the Narew lowland river reach. For this purpose, high resolution hydrologic and water quality time series have been used. Spectral analyses of time series using continuous wavelet transform scheme have been applied in order to identify characteristic scales, its duration, and localisation in time. The results of wavelet analysis have shown a great number of periodicities in time series at the inter-annual time scale when compared to the classical Fourier analysis. Additionally, wavelet coherence revealed the complex nature of the relationship between dissolved oxygen and hydrological variables dependent on the scale and localisation in time. Hence, the results presented in this paper may provide an alternative representation to a frequency analysis of time series.

Key words: dissolved oxygen, wavelet analysis, time series, lowland river.

1. INTRODUCTION

It is commonly known that a measure of organic waste load in rivers is biochemical oxygen demand BOD, which in general terms indicates the amount of oxygen drawn upon in the process of decomposition of the waste. The rate at which BOD is exerted combined with the rate at which oxygen is restored determines the level of dissolved oxygen (DO). Specific aspects of environmental water resources require the knowledge and understanding of the variability of oxygen levels in relation with water level fluctuations and river discharges. There are a variety of alternative methods to analyse the DO time series, including the most common method of Fourier analysis, but they often fail to show detailed temporal patterns. To avoid such problems, wavelet analysis has been frequently proposed to analyse numerous environmental signals but not much has been done in this respect for the studies of dissolved oxygen. This work is an extension of a recent study of Rajwa-Kuligiewicz *et al.* (2015), in which the time series of dissolved oxygen and water temperature coupled with meteorological and hydrological data obtained from two lowland rivers having contrasting hydrological settings have been examined in detail. It aims to analyse the variability of oxygen regime in a lowland, very natural river, and examine the role of the dominant hydrologic patterns on the inter-annual variability of rivers' oxygenation. In particular, we tried to identify the dominant scales of variation in time series. This has been done by the application of the wavelet transform which helps to identify the dominant modes of variability and their variation in time. The current work outlines the practical aspects of the so-called continuous wavelet transform (CWT) method, highlighting its relevance in time series analysis of eco-hydrological data.

The idea of the wavelet transform is to convolve the signal to be analysed with several oscillatory filter kernels representing different frequency bands, respectively (Kumar and Foufoula-Georgiou 1997). One of the most important advantages of the wavelet approach is the proportional relationship between bandwidth and frequency. Wavelet analysis has found numerous applications in science and engineering. For example, plenty of studies have been investigating the potential of using wavelet transform in the processing of seismic data (Chakraborty and Okaya 1995, Cheng *et al.* 2015, Zamani *et al.* 2014) and time series analysis of streamflow and precipitations (Carey *et al.* 2013, Coulibaly and Burn 2004, Kang and Lin 2007, Labat 2008, Lafrenière and Sharp 2003, Saco and Kumar 2000, Smith *et al.* 1998, Szolgayová *et al.* 2014, Venugopal *et al.* 2006, Zolezzi *et al.* 2009). Scanlon and Albertson (2001) applied wavelet transform to describe turbulent transport of carbon dioxide and water vapour within vegetation canopies. More recently, Kanani and da Silva (2015) considered the application of wavelets in the visualisation of coherent structures. The above studies are obviously not exhaustive and more examples will be presented later, while introducing the key components of continuous wavelet transform (CWT) method.

2. METHODS

2.1 Data

Data used in this study was obtained from the Narew River monitoring station (see Rajwa-Kuligiewicz *et al.* (2015) for a detailed description of the data). The Narew River is located in north-east Poland (see Fig. 1). Along the considered section the river valley is flat and swampy, and has a varying width from 250 m do 3.5 km. The majority of its bank retained a natural character; the river flows in several channels and meanders, forming a network of streams extending in the whole width of the valley. Data including water temperature, dissolved oxygen, and water level were evenly sampled at 1-hour time interval using multi-parameter sonde manufactured by Hydrolab (Fig. 2A). River discharge was taken from a gauging station in Suraż (Fig. 2B), whereas precipitations and short-wave radiation were taken from the meteorological station in Kurowo village (Fig. 2C-D). All data covering almost 3 years of continuous monitoring were treated collectively at 1-hour time interval. Data gaps resulting from occasional failures and maintenance of measuring devices were interpolated using linear interpolation.

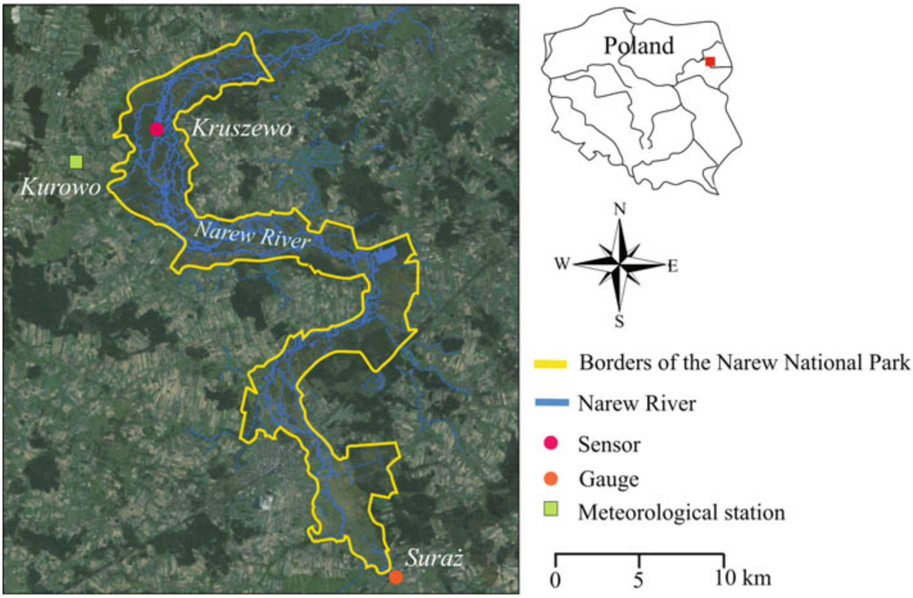

Fig. 1. Study site location.

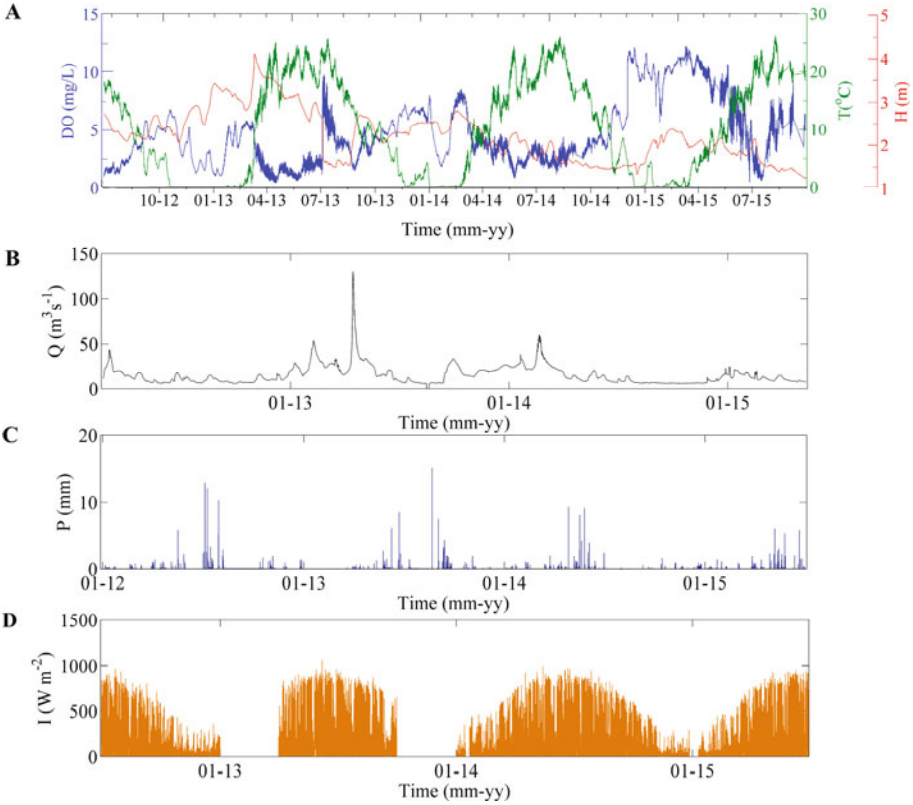

Fig. 2. Time series: (A) dissolved oxygen, water temperature, and water level time series (Kruszewo); (B) hydrograph (Suraż); (C) rainfall (Kurowo); and (D) shortwave radiation (Kurowo).

2.2 Wavelet data analysis

Wavelet analysis of time series has been applied in order to identify characteristic scales and its localisation in time. Wavelet transform decomposes the entire signal to the components called wavelets having different frequencies and analyses each segment of the signal with resolution fitted to its scale. In contrast to the windowed Fourier transform, the wavelet transform uses a changeable window size that narrows at high frequencies and widens at low frequencies. In our study we applied a continuous wavelet scheme as it is more robust to noise (Cazelles *et al.* 2008). Moreover, it is suitable for the analysis of geophysical and hydrological time series (Coulibaly and Burn 2004). Generally, the continuous wavelet transform is determined using discrete time series. However, in contrast to discrete wavelet transform, it can be computed for each scale. The CWT is also continuous with respect to displacement, which means that for a particular scale the wavelet is moved smoothly in the whole domain of the analysed function. For the sake of simplicity, only one-dimensional wavelet is considered herein. The continuous form of the wavelet transform (CWT) of a time series $f(t)$ can be expressed mathematically as:

$$F_{\mathrm{CWT}}\left(a,b\right)=\frac{1}{\sqrt{a}}\int_{-\infty}^{+\infty} f\left(t\right)\psi^{*}\left(\frac{t-b}{a}\right)dt \;, \tag{1}$$

where $F_{\mathrm{CWT}}\,(a, b)$ is a wavelet coefficient, ψ is a mother wavelet, and * denotes the complex conjugate form. Parameter a is a scaling factor reflecting the degree of dilatation or compression of the mother wavelet. It ensures that energy presented by each wavelet is independent of the scale. Parameter b is a translation in time corresponding to the location of the basic function in time t in the analysed signal. The mother wavelet has got a defined shape being compared to the analysed signal $f(t)$ by shifting in position (b – translation factor) and frequency (a – scale factor). It is also worth noting that each wavelet must have zero mean to satisfy the admissibility condition. This guarantees that the wavelet transform is invertible (Farge 1992, Farge *et al.* 2013, Daubechies 1990).

The results of the CWT are represented by a set of wavelet coefficients in the scale-space plane, which holds all information about the input signal. These coefficients are the function of scale and position and are a measure of correlation of the signal f with the wavelet. For the narrow wavelets (small scale) coefficients represent the content of high-frequency components, whereas for the wide wavelets (big scale) they represent the content of low-frequency components (Lau and Weng 1995, Kumar and Foufoula-Georgiou 1997). Due to the fact that more stretched wavelet is comparable with a signal in a wider range of its variability in time, the corresponding coefficients – transform values represent global information of the analysed signal. Consequently, the set of these coefficients for the particular scale corresponds to the set of approximation coefficients of the highest discrete level of wavelet expansion. By contrast, narrow wavelets enable the separation of fast-changing features in the signal. Given the above, the wavelet transform is a convenient method for the analysis of non-stationary time series and transient signals (Percival and Walden 2000).

In our studies we used the Morlet wavelet (Fig. 3, Eq. 2) as it is reasonably well localised in time and frequency (Cazelles *et al.* 2008, Grinsted *et al.* 2004, Daubechies 1990). The Morlet wavelet is often used for environmentally oriented signals. It is a complex conjugate ($b \in \mathbf{R}$, $a > 0$) incorporating the amplitude and phase of basic function. The phase in the wavelet transform is the same as the phase in the Fourier transform decomposition

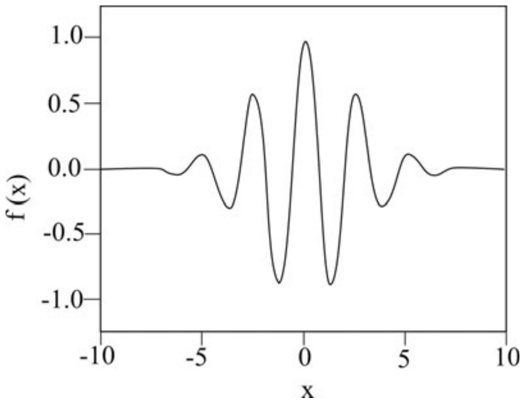

Fig. 3. The Morelet wavelet with $\omega_0 = 6$.

(Torrence and Compo 1998). Here, the frequency of oscillations and the width of the mother wavelet, except of the amplitude of wavelet, refer to the scale. The Morelet wavelet is presented in Fig. 3 and is defined by Eq. 2 as follows:

$$M_{\mathrm{Mor},0}\left(t\right) = e^{i\omega_0 t} e^{\left(-\frac{t^2}{2}\right)} , \tag{2}$$

where t is time, and ω_0 is the non-dimensional frequency which usually falls between 5 and 6. The continuous wavelet transform is calculated for a dyadic scale meaning that the proceeding values of the scale are the power of 2. The scale corresponds to the length of wavelet, *i.e.*, the number of time steps used for the CWT calculation.

Due to the finite-length of time series, errors are observed at the edges of the wavelet power spectrum. This happens because the wavelet is translated along the signal and the convolution is calculated for each time step and each scale. As a consequence, at the edges of the signal the convolution requires non-existing values beyond the boundary. This region is called the cone of influence. In this region the wavelet power drops to e^{-2} of the value at the edge (Torrence and Compo 1998). There are two approaches to deal with it, either accept the loss of data at boundaries of the signal and truncate these results, or apply an artificial extension of time series. So far, several methods of extension have been developed such as zero padding, periodic extension and symmetric extension (Keinert 2004). No matter which extension mode is applied, it introduces discontinuities at endpoints and decreases the amplitude in boundaries at larger scales. Therefore, rather than having false information, we truncated the results obtained at the edges.

Once the mother wavelet has been chosen, we calculated spectral characteristics of time series such as the global wavelet power spectrum, cross-wavelet transform and wavelet coherence for time series. By analogy with the Fourier power spectrum, wavelet power spectrum (WPS) is the wavelet transformation of the autocorrelation function. It represents the distribution of power not only in scale (frequency) as the Fourier transform does, but also in time. On the other hand, the cross-wavelet transform (WCS) enables the examination of the relationship between two signals in the time-scale plane. It can be decomposed into cross-wavelet power and phase, which shows the delay between two time series at particular time and scale. The amplitude of the cross-wavelet transform when normalised to the two single wavelet power spectra yields wavelet coherence (WTC), which describes a linear dependence of two signals for a given scale (Maraun and Kurths 2004). Thus, it can be interpreted as a correlation coefficient. The detailed description of aforementioned functions is provided in: Torrence and Compo (1998), Torrence and Webster (1999), and Grinsted *et al.* (2004). The calculations of wavelet functions were performed in Matlab using wavelet coherence script developed by Grinsted *et al.* (2004).

3. RESULTS AND DISCUSSION

3.1 Fourier power spectrum

As reported by Rajwa-Kuligiewicz *et al.* (2015) Fourier analysis of dissolved oxygen and water temperature time series indicated the existence of one peak in the power spectrum, which corresponds to the daily cycle. Moreover, power spectra of DO, water temperature, and water level time series can be roughly approximated by the "–1" slope. The fact that time series power spectrum exhibits $1/f$ scaling suggests the presence of self-similarity phenomenon, which manifests in the same pattern over different timescales. By contrast, precipitations time series can be approximated as white noise. Besides, the fact that the scaling may reflect some natural process such as the transport and storage of solutes within the catchment (Kirchner *et al.* 2004, Kirchner and Neal 2013), it may also be useful in the assessment of environmental variability among different ecosystems (Rajwa-Kuligiewicz *et al.* 2016).

3.2 Wavelet analysis

Figure 4 presents wavelet transform coefficients of dissolved oxygen time series. In here, higher scales represent more stretched wavelets corresponding to the low frequency ranges. Therefore, higher scales provide global information on a signal. This means also that lesser number of points characterise the signal. On the other hand, small scales represent more compressed wavelets reflecting high frequencies. Hence, small scales provide more detailed information of a hidden pattern in the signal (that lasts relatively short

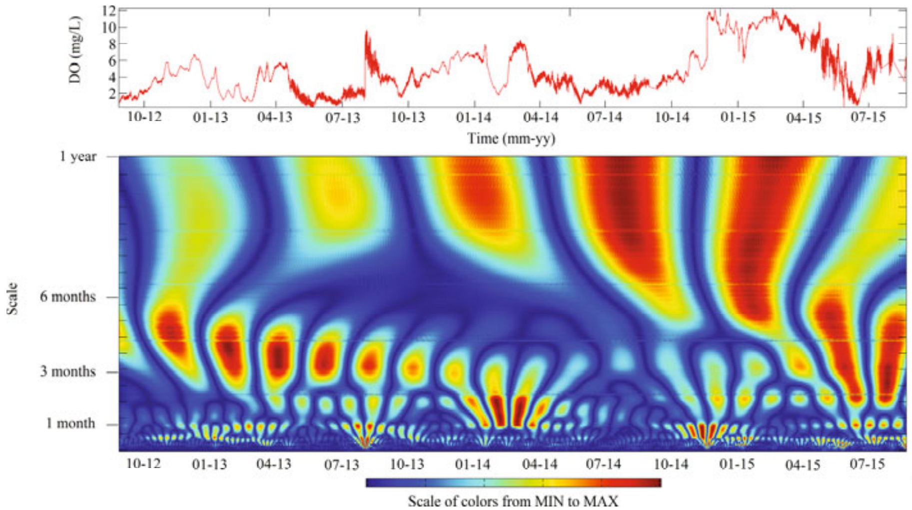

Fig. 4. The CWT coefficients for dissolved oxygen time series.

time). This means also that more samples corresponding to a smaller time interval characterise the signal. In short, when moving up the scale we stretch our wavelet, then we do a correlation of the wavelet with the signal, and obtain the second raw of the scalogram. This procedure is repeated several times depending on the number of scales.

Accordingly, Figs. 5-7 show the wavelet transform coefficients of the remaining time series, namely water temperature, water level, and streamflow. In Figs. 4-7 the presence of multiscale structures and their temporal locations are clearly visible. One can also see small-scale features within large-scale features. The colour indicates the value of the wavelet coefficient, and provides a measure of the relative amplitude of each point. The vertical dark blue lines represent places of rapid changes of the mean value (local minima of coefficients). Therefore, the transform can be used as a detector of sharp changes in the signal.

In the first row, related to the smallest scale, amplitudes are weak indicating that nothing in the signal correlates with the wavelet (Fig. 4). Smaller values of coefficient are especially visible in late summer of 2014. In dissolved oxygen time series (Fig. 4), the maximum peaks of amplitudes occur with periods of 1 month, 4 months, and 1 year. In 2014 the peaks are observed from January to April with a period of 1 month. In 2015 the highest peaks occurred in August and September with periods of about 3-4 months. The coefficients were higher when compared to previous years. The attenuation of oscillations from 4 to 6 months scale is visible from April 2013 till August 2014. It is also visible that DO time series show greater variability in

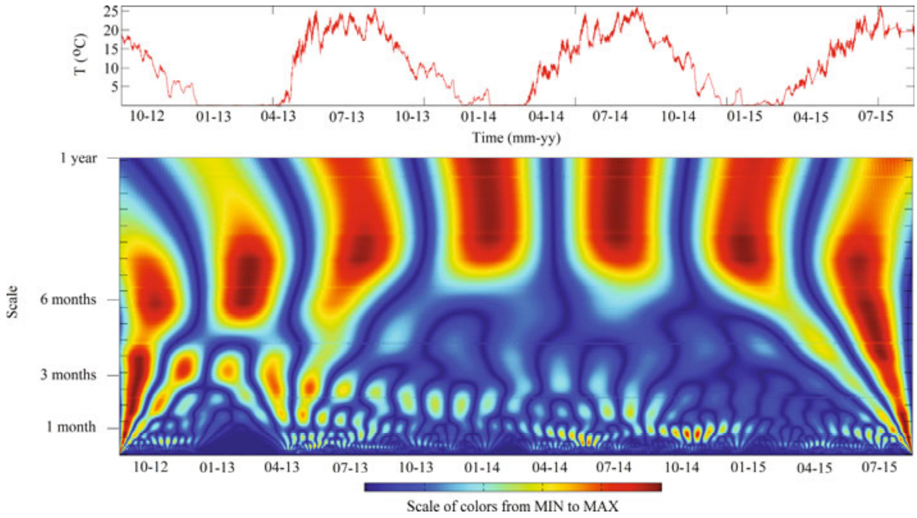

Fig. 5. The CWT coefficients for water temperature time series.

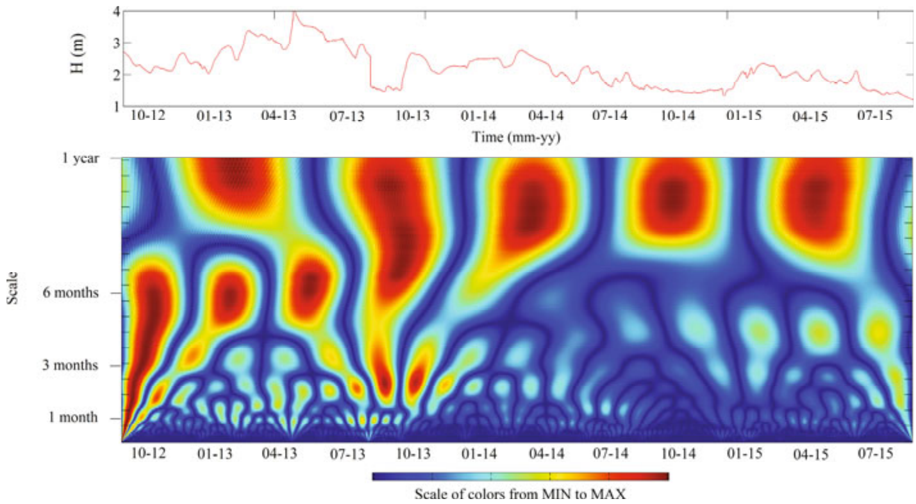

Fig. 6. The CWT coefficients for water level time series.

the value of wavelet coefficient at small scales when compared to other time series (Figs. 5-7).

Water temperature and its variability influence significantly water quality and river ecosystems (see, *e.g*., Kalinowska and Rowiński 2015). It controls solubility of dissolved oxygen, stream metabolism, and toxicity of pollutants (Demars *et al.* 2011). Figure 5 shows that the maximum values of wavelet coefficient for water temperature correspond to the period of 1 year.

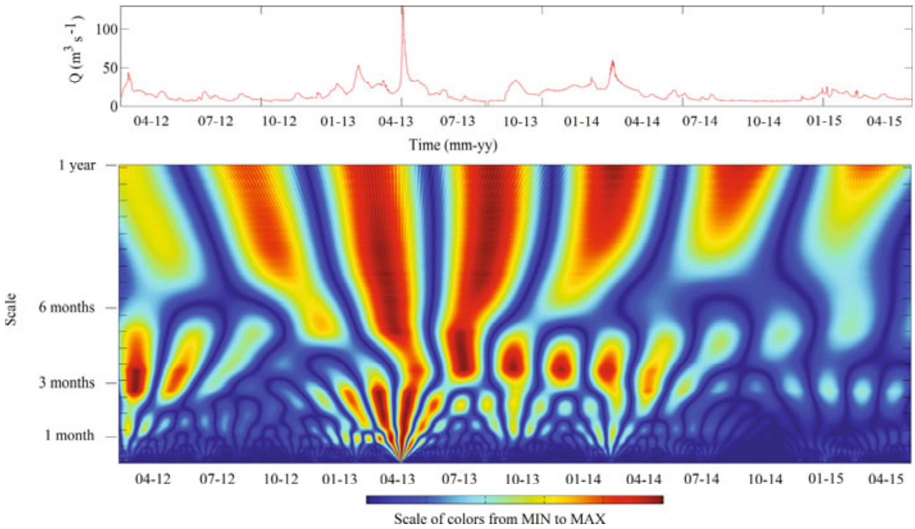

Fig. 7. The CWT coefficients for streamflow time series.

By contrast, the lowest amplitudes occur for the shorter periods (small scales) in winter and spring.

In water level time series (Fig. 6), higher coefficients are observed at the scale of 10 months. Some additional periodicities are visible at the scale of 6 months from the fall 2012 till April 2013 and at the scale of 2 months in late summer 2013. By comparison, in river discharge' time series (Fig. 7), the highest coefficients are observed in 2013 with periods of 1 and 3 months. It is also visible that the highest values of coefficients overlap with the discharge peaks.

3.3 Wavelet power spectrum

Wavelet power spectrum provides the information on the power density in time and scale, and thus enables the identification of dominant and characteristic scales of variations. Figures 8-12 present the global wavelet power spectra of time series. The right plot shows the contribution of a particular scale to the overall variability of the time series. It is visible that most of the power is concentrated within the 0.5-1 year band, although there is some appreciable power at shorter periods. Generally, the wavelet power spectra (WPS) of analysed time series have similar structure (the power is higher for a greater timescales) but the location of individual regions of high power are different for each WPS. The power varies not only across time at a given scale, but also among scales at particular time. All analysed time series have shown a strong annual temporal pattern. The comparison between the power

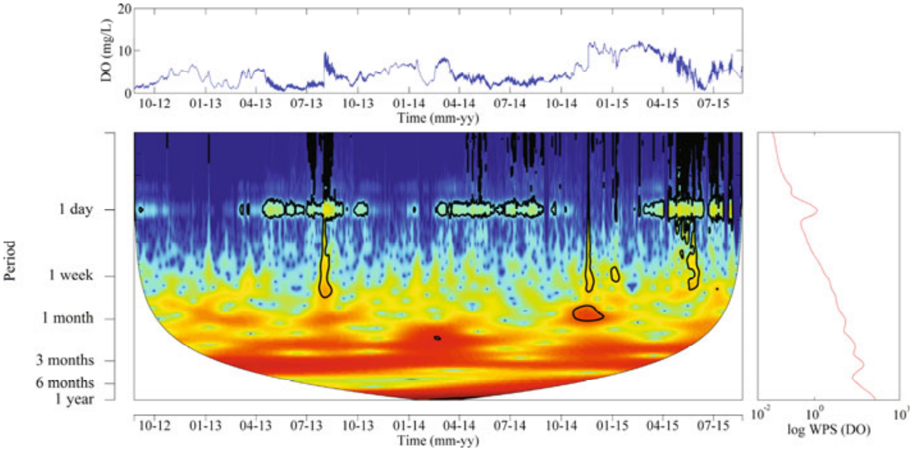

Fig. 8. Wavelet power spectrum of dissolved oxygen and mean power spectrum for each scale.

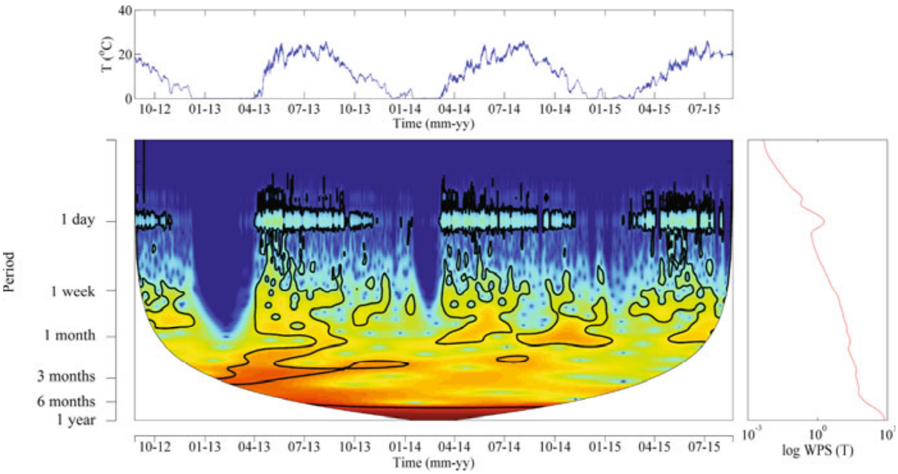

Fig. 9. Wavelet power spectrum of water temperature and mean wavelet power spectrum for each scale.

spectra of time series reveals some important discrepancies. For example, there is evidence that DO is highly localised at high frequencies (Fig. 8). However, the highest powers are observed at greater timescales. In here, the contour lines identify peaks of greater than 95% confidence for a red noise process with a lag of –1 (Torrence and Compo 1998). The cone of influence is presented as a white area located outside the wavelet power spectrum. It should also be noted that the area out of the WPS results not only from the noise but also, to a lesser extent, from the natural processes.

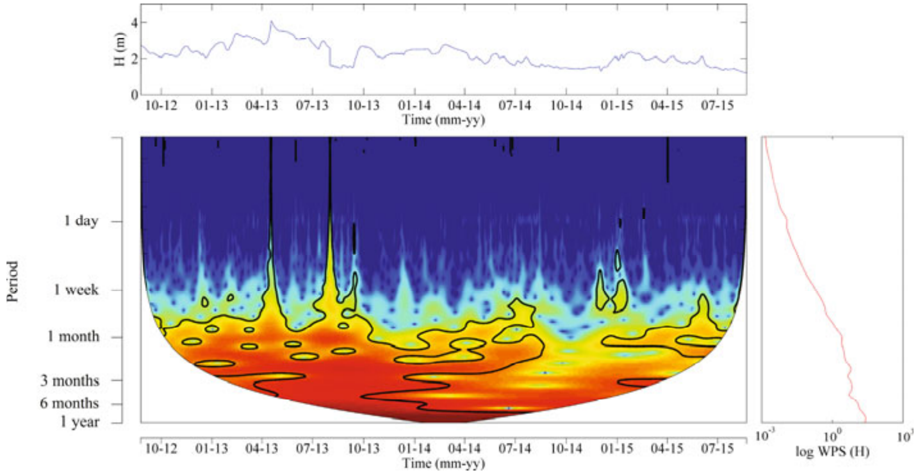

Fig. 10. Wavelet power spectrum of water level and mean wavelet power spectrum for each scale.

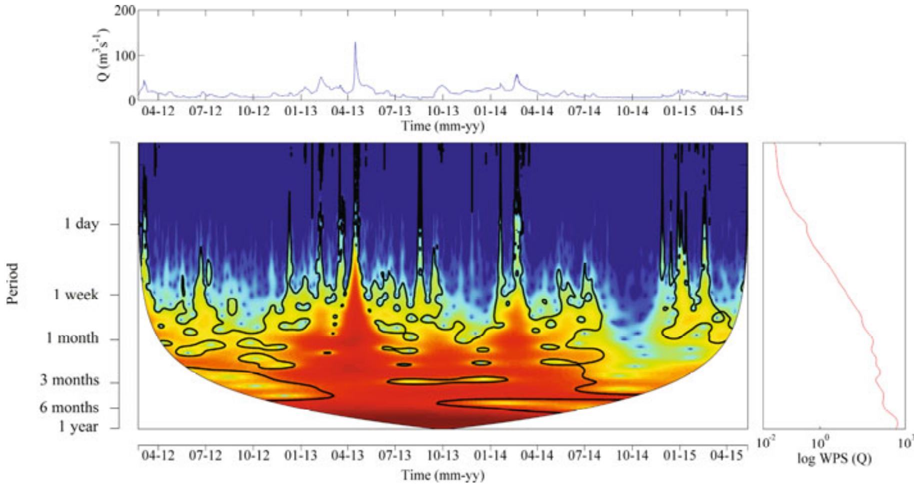

Fig. 11. Wavelet power spectrum of river discharge and mean wavelet power spectrum for each scale.

The dominant frequency (~1 day) in dissolved oxygen (Fig. 8) and water temperature (Fig. 9) time series is situated along the horizontal axis. As expected, daily cycle is characterised by relatively high-power content. It is also visible that the mode of variability vanishes during winter (Figs. 8 and 9). The daily periodicity in DO time series (Fig. 8) begins in March and prevails till November, which is associated with the greatest amplitudes of water temperature and intensified biological activity. This persistent band is oc-

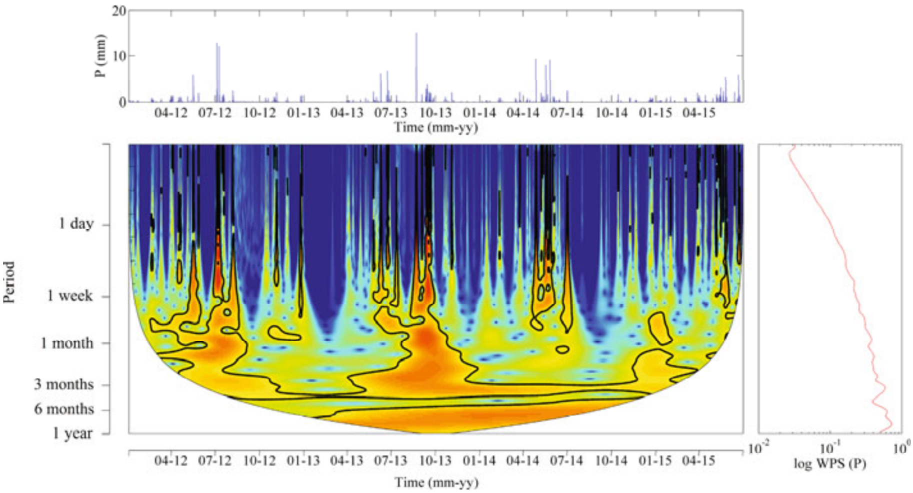

Fig. 12. Wavelet power spectrum of rainfall and mean wavelet power spectrum for each scale.

casionally interrupted by low powers, resulting from the rapid changes in hydro-meteorological conditions.

Strong daily cycle in water temperature (Fig. 9) is driven by the changes of air temperature and insolation. These oscillations are most evident in the warmer season of the year. Over the wintertime, no variability is observed. It is also visible that the WPS of water temperature exhibits far more inter-annual variability. A number of short-term temporal patterns can be detected at periods ranging from 1 week up to 1 month. These periods overlap with the short-term variations in streamflow.

The WPS of water level is more homogenous and displays low-frequency variability (Fig. 10). The most prominent periodicity occurs at the scale of 1 month and spans up to 1 year with small breaks. This pattern is visible for the whole analysed period, except of winter 2014/2015. In contrast to the water level WPS, the power distribution in the streamflow WPS (Fig. 11) is shifted to the higher frequencies (~3 days). It is also visible that river discharge exhibits large variations of wavelet power almost across whole timescales and becomes more variable at higher flow rates (Fig. 11). In autumn 2014 no significant pattern was displayed in water level and river discharge, which can be attributed to the exceptionally low flow and small rainfall.

In the wavelet power spectrum of rainfall, the dominant periodicity is observed at the scales of 4 months and 1 year (Fig. 12). The greatest powers overlap with periods of the highest rainfall observed in late summer. The exception was 2014 with the predominance of rainfall in the spring and early summer. These high rainfall periods are reflected by long spikes at that time location. A similar pattern can be observed for streamflow peaks (Fig. 11).

3.4 Cross-wavelet power

The cross-wavelet power reveals areas in the time-frequency space where the time series show a high common power, *i.e.*, they represent the local covariance between the time series at each scale. Figure 13A shows the cross-wavelet power of water temperature and dissolved oxygen. It is visible that water temperature and dissolved oxygen periodicities coincide at the scale of 1 day and 1 year. Arrows in this plot indicate the local relative phase between these two time series. The right direction of arrows at a daily scale suggests that time series are in phase. Moreover, it is easy to note that the ar-

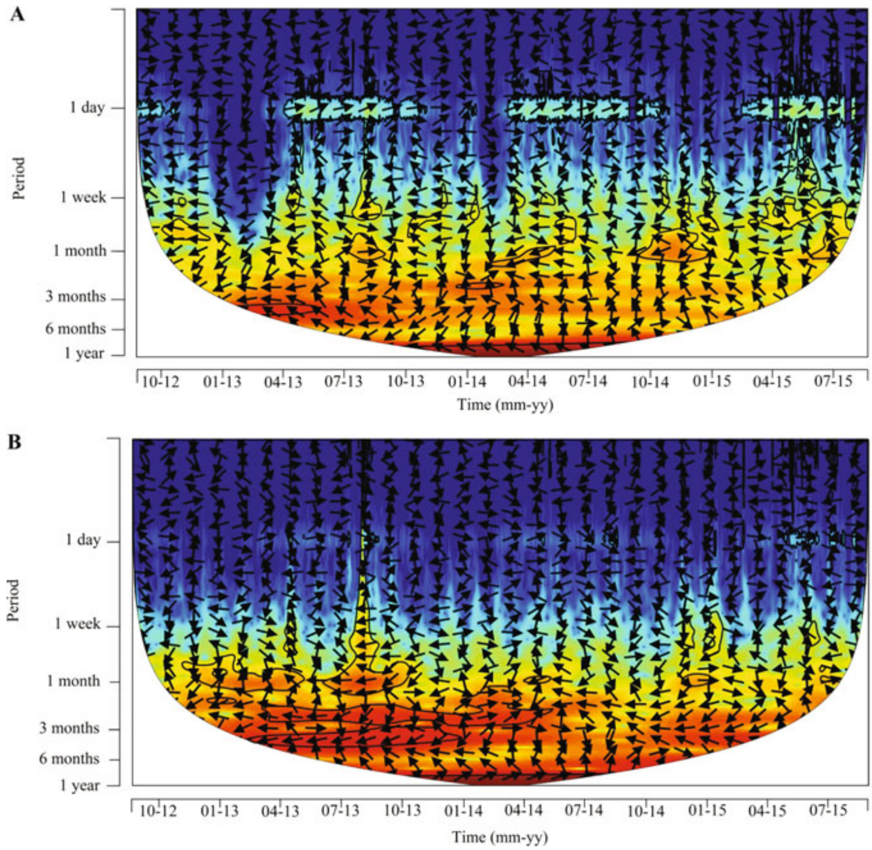

Fig. 13. Cross wavelet power: (A) of water temperature and dissolved oxygen, and (B) water level and dissolved oxygen.

rows slightly point downward implying that dissolved oxygen lags water temperature. For the higher scales (longer periods) arrows show an opposite direction, which means that time series are in anti-phase. It is also visible that DO wavelet power converges with water level at higher scales (Fig. 13B). It should be stressed, however, that the results obtained in this way can lead to the misleading interpretation since the cross-wavelet power is the product of two non-normalised spectra (Maraun and Kurths 2004). As the result, the estimated wavelet power spectrum will always be non-zero even if the true cross spectrum is zero. Moreover, the peaks may appear for two independent signals in the situations of covarying power or strong power of a single spectrum (Schaefli *et al.* 2007).

3.5 Wavelet coherence of dissolved oxygen and water temperature

Wavelet coherence overcomes the disadvantages of the cross-wavelet power spectrum since it shows the normalised dependence of two time series. Figure 14 displays the wavelet coherence between time series. Highly coherent areas indicate high values of the linear correlation. Arrows show the phase relationship between DO and water temperature time series.

Figure 14A shows that water temperature and dissolved oxygen time series are coherent around 1-day period band. This coherence is observed for a larger part of the year. Moreover, there are some red blobs elongated vertically from 3 days up to 1.5 month. The last coherent region occurs at the scale of 1 year. Despite the strong coupling at the daily and annual scales, there is a weak, or even no, coherency at the period from 1.5 month to 1 year. For shorter periods, the arrows point right, which means that dissolved oxygen is in phase with water temperature. It can be attributed to the responsive nature of DO since its solubility essentially depends on water temperature. Conversely, for longer periods the arrows point left, which implies that dissolved oxygen is in anti-phase with water temperature. This means that two time series are anti-correlated. It is also visible that some arrows slightly point down, indicating that two time series are out of phase and thus the correlation between them is non-linear. In this regard, down angle arrows indicate that DO lags water temperature by this specific angle which represents a fraction of the cycle at that period. From the pragmatic point of view, the wavelet coherence provides information on the relationship between water temperature and dissolved oxygen. Therefore, it might be useful in the modelling of time series. Based on the wavelet coherence one may decide whether the dependence can be described using a linear equation with lags, or requires the application of non-linear model with lags.

By comparison, Fig. 14B depicts the coherence between short-wave radiation and dissolved oxygen time series. A strong linear correlation is observed at periods of 12 hours, 1 day, and 1 year. As noted elsewhere, sunlight affects the photosynthesis rate and thus the production of oxygen by aquatic plants and algae. However, our results have shown that dissolved oxygen is less correlated with short-wave radiation over time than water temperature. In contrast to water temperature, short-wave radiation is more sensitive to cloud cover and the distance from the measuring point.

Figure 14C presents wavelet coherence between water level and water temperature time series. It is visible that water temperature is less coherent with water level than dissolved oxygen. In the coherence spectrum, one can distinguish two highly correlated periods. First is a daily period represented by red interrupted bulbs along the *x*-axis, which are followed by low-power periods. The second is the annual period. Moreover, several statistically sig-

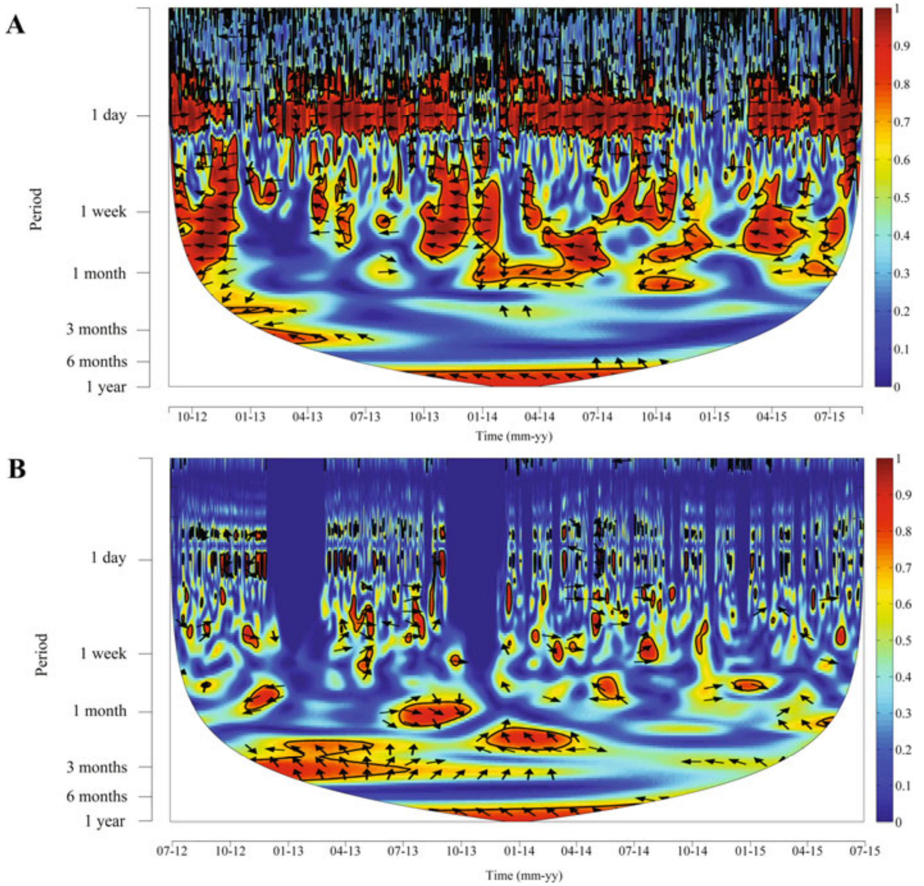

Fig. 14. Caption on next page.

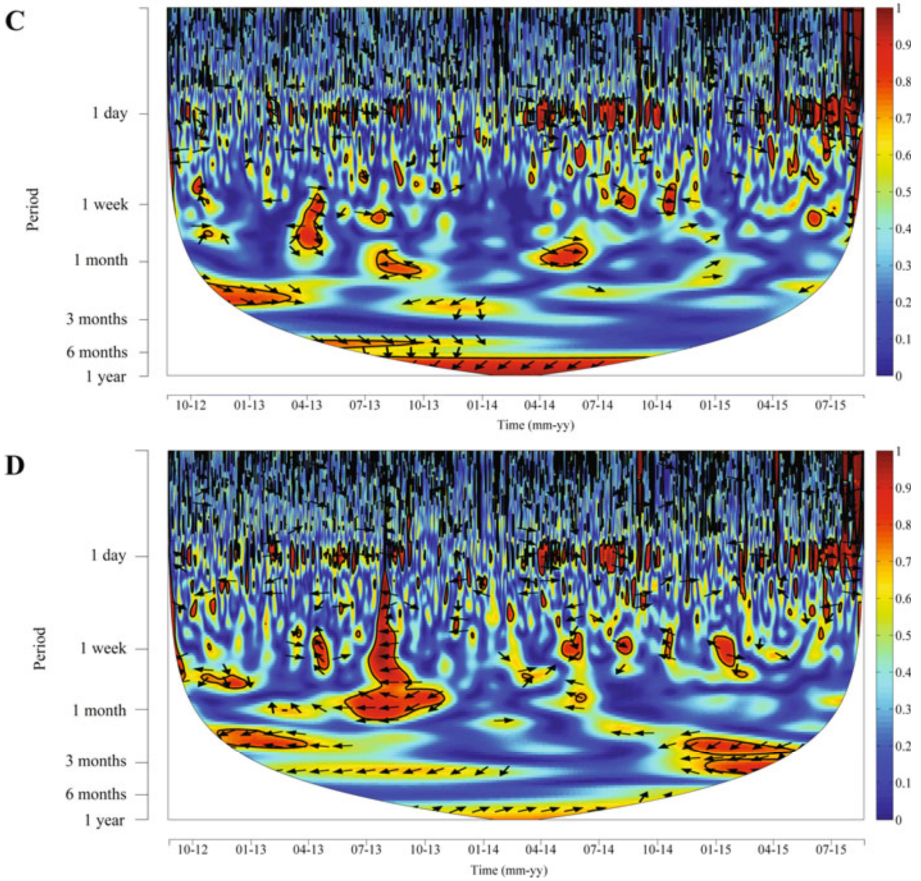

Fig. 14. Wavelet coherence: (A) water temperature and dissolved oxygen, (B) insolation and dissolved oxygen, (C) water level and water temperature, and (D) water level and dissolved oxygen time series.

nificant peaks occur at the period of about 3 days up to 1.5 month. The arrows' directions seem to be randomly distributed in the coherence spectrum among all scales, except the annual scale, where the phase is represented by leftward angle arrows. This indicates that water temperature is anti-correlated with water level.

Figure 14D displays wavelet coherence between water level and dissolved oxygen wavelet power spectra. As visible, those two time series are poorly correlated. However, high coherence can be observed in a narrow band at a daily timescale. Moreover, small individual peaks are visible at the period of one week. In fact, this consistency has not been reported in the earlier work of Rajwa-Kuligiewicz *et al.* (2015) since both, the statistical method and Fourier technique, failed to show that. Interestingly, high coherence occurs during flood events, suggesting that extreme events such as floods directly affect the river ecosystems. As noted by Marion *et al.* (2014) these events may not only disturb the river' habitats but also introduce changes in existing ecological states.

4. CONCLUSIONS

In this study we used wavelet analysis to asses dissolved oxygen regime over a wide range of temporal scales ranging from sub-daily to annual. Similarly, time series of temperature, water level, and discharge were treated. Wavelet analysis has shown better performance in detecting detailed temporal patterns in non-stationary time series compared with the conventional Fourier analysis. Our results have shown that the wavelet technique helps to elucidate a greater number of periodicities in time series. Moreover, it facilitates the comparison of two time series and identification of highly correlated periods in both time series. From a pragmatic point of view, it helps to determine what kind of factors influences oxygen regime, when the impact is significant and how long it lasts.

Acknowledgments. This research was supported by the Ministry of Science and Higher Education within statutory activities 3841/E-41/S/2016. Agnieszka Rajwa-Kuligiewicz gratefully acknowledges the financial support from the Interdisciplinary Polar Studies. The authors are very grateful to the two reviewers for their constructive comments, which helped to improve the manuscript.

References

Carey, S.K., D. Tetzlaff, J. Buttle, H. Laudon, J. McDonnell, K. McGuire, J. Seibert, C. Soulsby, and J. Shanley (2013), Use of color maps and wavelet coherence to discern seasonal and interannual climate influences on streamflow variability in northern catchments, *Water Resour. Res.* **49**, 10, 6194-6207, DOI: 10.1002/wrcr.20469.

Cazelles, B., M. Chavez, D. Bertaux, F. Ménard, J.O. Vik, S. Jenouvrier, and N.C. Stenseth (2008), Wavelet analysis of ecological time series, *Oecologia* **156**, 2, 287-304, DOI: 10.1007/s00442-008-0993-2.

Chakraborty, A., and D. Okaya (1995), Frequency-time decomposition of seismic data using wavelet-based methods, *Geophysics* **60**, 6, 1906-1916, DOI: 10.1190/1.1443922.

Cheng, B., T. Xu, B. Robbins, and Z. Shen (2015), Reef reservoir identification by wavelet decomposition and reconstruction: A case study from Yuanba gas field in China, *Acta Geophys*. **63**, 4, 1025-1043, DOI: 10.1515/acgeo-2015-0028.

Coulibaly, P., and D.H. Burn (2004), Wavelet analysis of variability in annual Canadian streamflows, *Water Resour. Res*. **40**, 3, W03105, DOI: 10.1029/2003WR002667.

Daubechies, I. (1990), The wavelet transform, time-frequency localization and signal analysis, *IEEE Trans. Inform. Theory* **36**, 5, 961-1005, DOI: 10.1109/18.57199.

Demars, B.O.L., J.R. Manson, J.S. Ólafsson, G.M. Gíslason, R. Gudmundsdóttir, G. Woodward, J. Reiss, D.E. Pichler, J.J. Rasmussen, and N. Friberg (2011), Temperature and metabolic balance of streams, *Freshw. Biol*. **56**, 6 1106-1121, DOI: 10.1111/j.1365-2427.2010.02554.x.

Farge, M. (1992), Wavelet transforms and their applications to turbulence, *Ann. Rev. Fluid Mech.* **24**, 395-458, DOI: 10.1146/annurev.fl.24.010192.002143.

Farge, M., K. Schneider, O. Pannekoucke, and R. Nguyen van yen (2013), Multiscale representations: fractals, self-similar random processes and wavelets, **In:** H.J.S. Fernando (ed.), *Handbook of Environmental Fluid Dynamics*, Vol. 2, CRC Press/Taylor & Francis Group, Boca Raton, 311-333.

Grinsted, A., J.C. Moore, and S. Jevrejeva (2004), Application of the cross wavelet transform and wavelet coherence to geophysical time series, *Nonlin. Process. Geophys*. **11**, 5/6, 561-566, DOI: 10.5194/npg-11-561-2004.

Kalinowska, M.B., and P.M. Rowiński (2015), Thermal pollution in rivers – modelling of the spread of thermal plumes. **In:** P. Rowiński and A. Radecki-Pawlik (eds.), *Rivers – Physical, Fluvial and Environmental Processes*, GeoPlanet: Earth and Planetary Sciences, Springer Int. Publ., 591-613, DOI: 10.1007/978-3-319-17719-9_24.

Kanani, A., and A.M. Ferreira da Silva (2015), Application of continuous wavelet transform to the study of large-scale coherent structures, *Environ. Fluid Mech.* **15**, 6, 1293-1319, DOI: 10.1007/s10652-015-9428-x.

Kang, S., and H. Lin (2007), Wavelet analysis of hydrological and water quality signals in an agricultural watershed, *J. Hydrol.* **338**, 1-2, 1-14, DOI: 10.1016/j.jhydrol.2007.01.047.

Keinert, F. (2004), *Wavelets and Multiwavelets*, Chapman & Hall/CRC Press, Boca Raton, London.

Kirchner, J.W., and C. Neal (2013), Universal fractal scaling in stream chemistry and its implications for solute transport and water quality trend detection, *Proc. Natl. Acad. Sci. USA* **110**, 30, 12213-12218, DOI: 10.1073/pnas.1304328110.

Kirchner, J.W., X. Feng, C. Neal, and A.J. Robson (2004), The fine structure of water-quality dynamics: the (high-frequency) wave of the future, *Hydrol. Process*. **18**, 7, 1353-1359, DOI: 10.1002/hyp.5537.

Kumar, P., and E. Foufoula-Georgiou (1997), Wavelet analysis for geophysical applications, *Rev. Geophys*. **35**, 4, 385-412, DOI: 10.1029/97RG00427.

Labat, D. (2008), Wavelet analysis of the annual discharge records of the world's largest rivers, *Adv. Water Resour*. **31**, 1, 109-117, DOI: 10.1016/j.advwatres.2007.07.004.

Lafrenière, M., and M. Sharp (2003), Wavelet analysis of inter-annual variability in the runoff regimes of glacial and nival stream catchments, Bow Lake, Alberta, *Hydrol. Process*. **17**, 6, 1093-1118, DOI: 10.1002/hyp.1187.

Lau, K.M., and H. Weng (1995), Climate signal detection using wavelet transform: How to make a time series sing, *Bull. Am. Meteorol. Soc*. **76**, 12, 2391-2402, DOI: 10.1175/1520-0477(1995)076<2391:CSDUWT> 2.0.CO;2.

Maraun, D., and J. Kurths (2004), Cross wavelet analysis: significance testing and pitfalls, *Nonlin. Process. Geophys.* **11**, 4, 505-514, DOI: 10.5194/npg-11-505-2004.

Marion, A., V. Nikora, S. Puijalon, T. Bouma, K. Koll, F. Ballio, S. Tait, M. Zaramella, A. Sukhodolov, M. O'Hare, G. Wharton, J. Aberle, M. Tregnaghi, P. Davies, H. Nepf, G. Parker, and B. Statzner (2014), Aquatic interfaces: a hydrodynamic and ecological perspective, *J. Hydraul. Res*. **52**, 6, 744-758, DOI: 10.1080/00221686.2014.968887.

Percival, D.B., and A.T. Walden (2000), *Wavelet Methods for Time Series Analysis*, Cambridge Series in Statistical and Probabilistic Mathematics, Cambridge University Press, Cambridge, DOI: 10.1017/CBO9780511841040.

Rajwa-Kuligiewicz, A., R.J. Bialik, and P.M. Rowiński (2015), Dissolved oxygen and water temperaturę dynamics in lowland rivers over various timescales, *J. Hydrol. Hydromech*. **63**, 4, 353-363, DOI: 10.1515/johh-2015-0041.

Rajwa-Kuligiewicz, A., R.J. Bialik, and P.M. Rowiński (2016), Spatio-temporal variability of water temperature in an anastomosing section of the Narew river. **In:** *Proc. 11th Int. Symp. Ecohydraulics, 7-12 February 2016, Melbourne, Australia*, Paper 26204.

Saco, P., and P. Kumar (2000), Coherent modes in multiscale variability of streamflow over the United States, *Water Resour. Res*. **36**, 4, 1049-1067, DOI: 10.1029/1999WR900345.

Scanlon, T.M., and J.D. Albertson (2001), Turbulent transport of carbon dioxide and water vapor within a vegetation canopy during unstable conditions: Identification of episodes using wavelet analysis, *J. Geophys. Res*. **106**, D7, 7251-7262, DOI: 10.1029/2000JD900662.

Schaefli, B., D. Maraun, and M. Holschneider (2007), What drives high flow events in the Swiss Alps? Recent developments in wavelet spectral analysis and their application to hydrology, *Adv. Water Resour*. **30**, 12, 2511-2525, DOI: 10.1016/j.advwatres.2007.06.004.

Smith, L.C., D.L. Turcotte, and B.L. Isacks (1998), Stream flow characterization and feature detection using a discrete wavelet transform, *Hydrol. Process*. **12**, 2, 233-249, DOI: 10.1002/(SICI)1099-1085(199802)12:2<233::AID-HYP 573>3.0.CO;2-3.

Szolgayová, E., J. Arlt, G. Blöschl, and J. Szolgay (2014), Wavelet based deseasonalization for modelling and forecasting of daily discharge series considering long range dependence, *J. Hydrol. Hydromech*. **62**, 1, 24-32, DOI: 10.2478/johh-2014-0011.

Torrence, C., and G.P. Compo (1998), A practical guide to wavelet analysis, *Bull. Am. Meteorol. Soc.* **79**, 1, 61-78, DOI: 10.1175/1520-0477(1998)079<0061:APGTWA>2.0.CO;2.

Torrence, C., and P.J. Webster (1999), Interdecadal changes in the ENSO-monsoon system, *J. Climatol*. **12**, 8, 2679-2690, DOI: 10.1175/1520-0442(1990)012<2679: ICITEM>2.0.CO;2.

Venugopal, V., S.G. Roux, E. Foufoula-Georgiou, and A. Arneodo (2006), Revisiting multifractality of high-resolution temporal rainfall using a wavelet-based formalism, *Water Resour. Res*. **42**, 6, W06D14, DOI: 10.1029/2005WR004489.

Zamani, A., A.P. Kolahi Azar, and A.A. Safavi (2014), Wavelet-based multifractal analysis of earthquakes temporal distribution in Mammoth Mountain volcano, Mono County, Eastern California, *Acta Geophys*. **62**, 3, 585-607, DOI: 10.2478/s11600-013-0184-3.

Zolezzi, G., A. Bellin, M.C. Bruno, B. Maiolini, and A. Siviglia (2009), Assessing hydrological alternations at multiple temporal scales: Adige River, Italy, *Water Resour. Res*. **45**, 12, W12421, DOI: 10.1029/2008WR007266.

Received 13 Fabruary 2016
Received in revised form 28 April 2016
Accepted 17 May 2016